microplastics

MDPI

Article

Improving Microspectroscopic Microplastic Data Extrapolation: From Field of View to Full Sample, and from Fragment 2D-Morphology to Mass

Oskar Hagelskjær [1,2,*], Henar Margenat [1,2], Nadiia Yakovenko [1,3], Gaël le Roux [2] and Jeroen E. Sonke [3,*]

[1] Microplastic Solution, Castanet-Tolosan, 31320 Toulouse, France; henar@microplasticsolution.com (H.M.)
[2] Centre de Recherche sur la Biodiversité et l'Environnement (CRBE-UMR5300), Université de Toulouse, Toulouse INP, CNRS, IRD, CRBE, 31326 Toulouse, France; gael.le-roux@cnrs.fr
[3] Géosciences Environnement Toulouse, CNRS UMR5563-IRD UR 234, Université Toulouse III-Paul Sabatier (UT3), 14 Avenue Edouard Belin, 31400 Toulouse, France
* Correspondence: oskar@microplasticsolution.com (O.H.); jeroen.sonke@get.omp.eu (J.E.S.)

Abstract

Microplastic (MP) analysis via microspectroscopy typically examines only 1–10% of filter substrates due to time constraints, requiring reliable extrapolation methods for quantitative environmental monitoring. Current subsampling strategies suffer from heterogeneous particle dispersion, leading to 50–80% error in MP quantification. Additionally, MP researchers require enhanced environmental MP mass datasets, necessitating reliable conversion algorithms from two-dimensional morphological data to mass estimates. This study introduces an area-based extrapolation technique for organic rich samples that compares the MP-to-generic particle area ratio within a rectangular field of view against total particle area on the entire filter membrane, combined with a simplified fragment morphology-to-mass conversion model (SFMM). First, two *Sphagnum* moss samples were analyzed using Raman microspectroscopy and critical angle darkfield illumination microscopy. The results demonstrated stable MP concentrations (17% RSD [n = 8]) despite heterogeneous generic particle distribution (31% RSD [n = 8]), with mean particle-area coverage of 2.4% per subsample. Then, twenty EasyMP^{TM} fragment reference materials (10 µm to 1500 µm), of known composite mass, were used to calibrate two different volume (V) expressions, one based on analyzed particle area (A) and minimum Feret diameter (F_{Min}, i.e., width), yielding $V = 0.34 \times F_{Min} \times A$. A second more approximate expression based on only the maximum Feret diameter (F_{Max}, i.e., length) yielded $V = 0.097 \times (F_{Max})^3$. These methods enable MP quantification and mass estimation from limited spectroscopic analysis.

Keywords: Raman microspectroscopy; environmental monitoring; particle distribution; mass estimation; subsample-analysis

check for updates

Academic Editor: Nicolas Kalogerakis

Received: 14 July 2025
Revised: 2 October 2025
Accepted: 9 October 2025
Published: 28 October 2025

Citation: Hagelskjær, O.; Margenat, H.; Yakovenko, N.; le Roux, G.; Sonke, J.E. Improving Microspectroscopic Microplastic Data Extrapolation: From Field of View to Full Sample, and from Fragment 2D-Morphology to Mass. *Microplastics* **2025**, *4*, 80. https://doi.org/10.3390/microplastics4040080

Copyright: © 2025 by the authors. Licensee MDPI, Basel, Switzerland. This article is an open access article distributed under the terms and conditions of the Creative Commons Attribution (CC BY) license (https://creativecommons.org/licenses/by/4.0/).

1. Introduction

Microplastics (MPs) are synthetic polymer particles that measure between 1 µm and 5 mm on their largest axis. When conducting microspectroscopic analysis for quantitative identification of MPs in the smallest size range, often only a small percentage of the filter substrate can be examined due to time constraints [1–3]. Even when n > 20,000 individual particles are analyzed over a 24 h period using Raman microspectroscopy, only 2–3% of the total filter area can be investigated [4,5]. Current Raman microspectroscopy subsampling strategies measure about 1 to 10% of the filter area [6].

Simplified extrapolation based on upscaling the analyzed fraction of a rectangular field of view (FOV) is unprecise because particle dispersion on a filter membrane is often heterogenous [6,7]. To correct for heterogenous particle dispersion by collecting data that is representative of the complete filter membrane, spectral acquisition techniques including wedge-shaped analysis [1], random particle selection [8] as well as spirals and crosses [9], have been developed. These methods all rely on adjusting data-sampling parameters to achieve statistically reliable MP content extrapolation based solely on the analyzed fraction.

However, particle count extrapolation represents only one component of comprehensive MP number concentration analysis. While accurate extrapolation of MP particle numbers addresses one analytical challenge, reliable conversion methods from morphological data to mass estimates are essential for comprehensive environmental monitoring [10–12]. Thermo-analytical methods such as pyrolysis GC/MS is able to provide direct MP mass concentrations for select polymers, but without quantification of MP size, and is therefore highly complementary to micro-spectroscopy. Because spectroscopic techniques dominate current MP analysis workflows [13–15], reliable conversion formulas that transform two-dimensional morphological data into mass estimates are needed. Most existing models estimate the volume of a particle by assuming a known three-dimensional geometric shape based on observed metrics such as area and size [16–19]. However, the irregular nature of environmental MP fragments makes it challenging to apply standardized geometric models consistently across diverse samples.

To address these issues, we present two novel approaches for particle count extrapolation and conversion from counts to mass. First, we developed a novel extrapolation approach that compares the ratio of generic particle area to MP distribution, within a single rectangular FOV against the total generic particle area across the complete filter membrane. Second, we present a Simplified Fragment Mass Model (SFMM) model to calculate the volume of small MP particles in the 10–1500 µm range using two observable parameters: (i) surface area, and (ii) minimum Feret diameter. The conversion formula uses a constant multiplier value to determine particle height, calibrated on observations presented in this study. This simple model relies on the principle that for a three-dimensional detached object perceived in two dimensions, the observed lateral dimensions (y- and x-axis) are likely superior in length, in comparison to the forward direction (z-axis) when the particle is in a resting state. This is because the gravitational force guides the particle towards a state of stable equilibrium, which is unlikely to be the shortest dimension [20], unless otherwise affected by surface adhesion not accounted for in this study. Because published MP studies typically report the distribution of particle length, but not width or area, we also calibrate our volume expression for MP length alone.

These two combined methodologies aim to enable accurate extrapolation of MP counts and mass conversion from limited spectroscopic analysis of small FOVs, facilitating efficient analysis of large environmental sample sets while maintaining analytical precision and reducing time constraints inherent to current microspectroscopic workflows.

2. Methods and Materials

2.1. Particle-Area Based Extrapolation

2.1.1. Experimental Setup

Two *Sphagnum* moss samples collected in France (sample-A and sample-B, respectively), were manipulated according to the complete purged air-assisted digestion and density separation protocol [5]. The final MP-enriched analyte was vacuum filtered onto two individual aluminium oxide filter membranes [pore size: 0.1 µm, filter diameter: 25 mm] (Anodisc, Whatman, Buckinghamshire, UK). The diameter of the filtered area was restricted by the width of the glass filtration funnel, measuring 14 mm in diameter. On each

of the two filter membranes, four individual 4 mm^2 square FOVs were analyzed by Raman microspectroscopy, following the pattern visualized in Figure 1. Between the individual samples, the total number and surface area of MPs and generic particles, as well as the relative size and polymer type distributions within the four FOVs were compared.

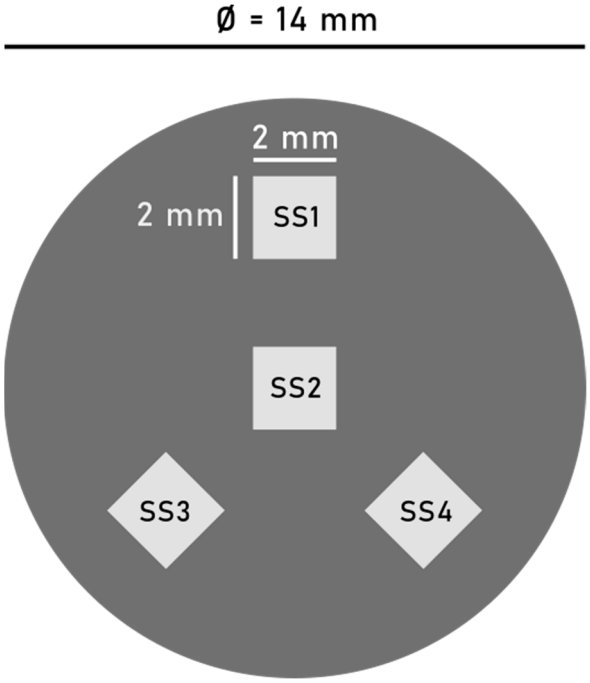


Figure 1. Visual representation of the distribution pattern of the four investigated 4 mm^2 FOVs on the filter area, in true relative scale. Graphic made with Inkscape V. 1.4.2.

2.1.2. Raman Microspectroscopy

A 4 mm^2 square FOV was analyzed by stitching 1666 micrographs into a high-resolution mosaic at a spatial resolution of 0.3 µm/pixel (effectively ~1 µm due to the fundamental refraction limit of visible light). Particles measuring $\geq$ 2 µm in area-equivalent diameter (circular model) were subject to µRaman analysis. Measurements were carried out at 20 °C using a Horiba LabRAM Soleil (Horiba Jobin Yvon, Paris, France). The samples were excited at 8% (7.2 mW) power output with a high stability air-cooled He–Cd 532 nm laser diode utilizing a Nikon LV-NUd5 100× objective (Nikon, Tokyo, Japan). The lateral resolution of the unpolarized confocal laser beam was on the order of 1 µm. Spectra were generated in the range of 200–3400 cm^{-1} using a 600 grooves/cm grating with a 100 µm split. The spectral resolution was on the order of 1 cm^{-1}. Particles within each mosaic, constructed using the LabSpec6 (LS6) SmartView configuration, were analyzed using the Particle Finder application V2. LS6 SmartView determines the topography (±50 µm) and saves the focal point of all particles on the captured micrograph, enabling the stage to rapidly move the relevant particle into focus. The micrograph is converted into an 8-bit 0–255 greyscale image in which parameters are set by the user to visually separate particles from the darker filter substrate. Each particle was analyzed for 1 s by 2 accumulations at the above-described settings.

2.1.3. Spectral Matching and Verification

Using the Spectragryph spectral analysis software V1.2.17d (Dr. Friedrich Menges SoftwareEntwicklung, www.effemm2.de/spectragryph (accessed on 1 February 2025)), all raw spectra were processed using adaptive baseline correction with 15% coarseness. The processed spectra were cross-referenced for their entire spectral range, using our in-house library containing selected spectra from the SLoPP and SLoPP-E [21] and the

Cabernard [22] spectral libraries, also including self-obtained in-house polymer spectra. Spectral matches were denominated by hit quality index (HQI)-values from 0 to 100% match. Spectra rated above 65% HQI were considered MP candidates and were manually inspected and sorted by a trained interpreter to determine their validity. Additionally, unintentionally partitioned MP particles (edge particles) were merged using a dedicated merging tool [4].

2.1.4. Full-Filter Particle-Area Estimation

Critical angle darkfield illumination (CADFLI) microscopy (ColSpec® MK2, Light-Form, Inc., Asheville, NC, USA) was used to capture multiple micrographs at a spatial resolution of 2.6 µm/pixel. 28 micrographs were merged using the Grid/collection stitching tool [23] to construct mosaics displaying the entire filter membrane. CADFLI microscopy enables the visual elimination of the filter substrate to isolate the residual particles, providing an effective means of estimating the total particle-area on the filter membrane (Figure 2).

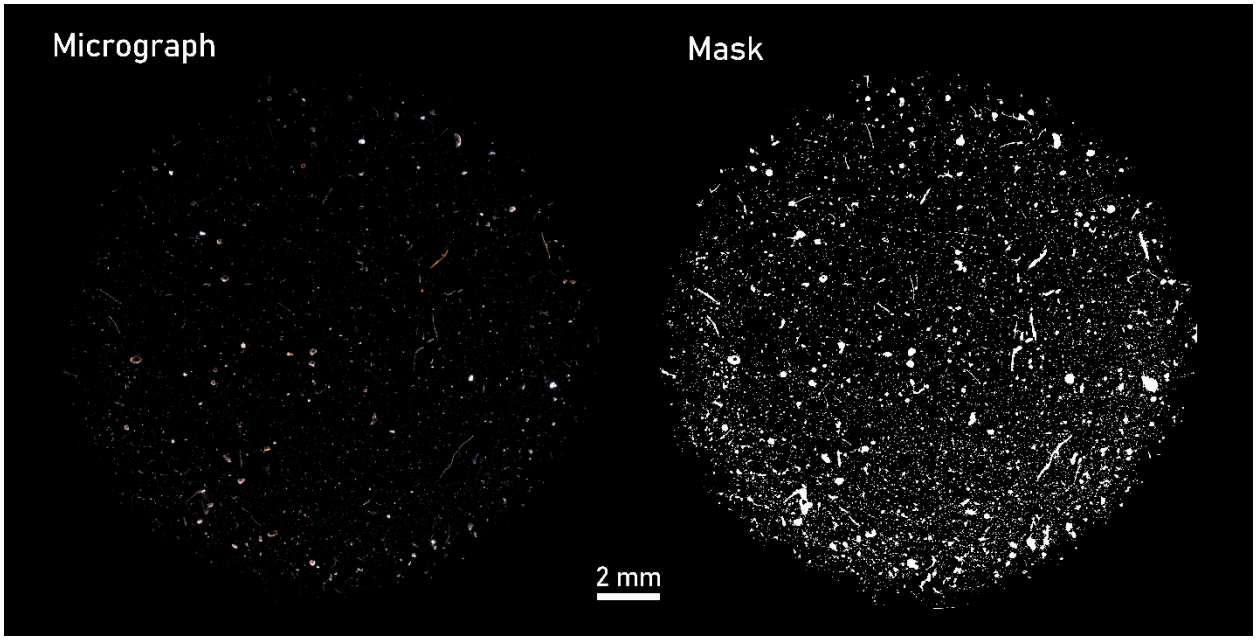


Figure 2. Micrograph mosaic captured under darkfield illumination depicting sample-B. 'Mask' refers to a masked version of the same image where all defined particles have been highlighted.

2.2. Two-Dimensional Particle Morphology to Mass Conversion Model

2.2.1. Experimental Setup

The following EasyMP™ fragment reference materials, produced through cryomilling and cascade sieving [24,25] in dry, neat (powder) format (EasyMP™, Microplastic Solution, Toulouse, France) were used in this experiment:

- Sample 1: polystyrene (PS) (500–1500 µm), Blue.
- Sample 2: polypropylene (PP) (100–500 µm), Red.
- Sample 3: polyethylene (PE) (10–200 µm), Blue.
- Sample 4: polypropylene (PP) (10–200 µm), Clear/transparent.
- Sample 5: polyethylene (PE) (10–100 µm), Green.

All data is available in the Supporting Information File S1 (SI1). For each sample, four subsamples were prepared. The total dry mass of each sample was determined using a PCE-ABT 220L balance (PCE instruments, Meschede, Germany). The dry mass of samples 2–5 were determined at 52.1 mg, 9.8 mg, 3.8 mg, and 5.4 mg, respectively. The powders

were weighed in glass pipette bottles (Oputec, Bendorf, Germany) and were suspended in either 30, 50- or 100 mL ethanol (95 vol.%), adapted to the quantity of MP powder to avoid filter saturation. For each sample, four subsamples between 0.5 and 1.0 mL were pipetted onto 25 mm filter membranes to capture photomicrographs via CADFLI microscopy. The mass of individual subsamples followed the current logic, using sample 2 as an example:

Dry MP powder mass: 52.1 mg (52,100 µg) → MP Powder suspended in 50 mL ethanol (95 vol.%) solution → 1 mL solution containing 1042 µg MP powder (52,100 µg/50 = 1042 µg) filtered onto 25 mm membrane for CADFLI microscopic analysis.

The applied dosing method represents a mean relative standard deviation (RSD) of 10% (n = 5) [24] not accounted for in this study. The comparatively larger particle size range of sample 1 allowed for the weighing of individual subsamples, where subsamples 1–4 weighed 17.4 mg, 20.4 mg, 14.0 mg, and 23.4 mg, respectively.

2.2.2. Particle Segmentation and Mass Conversion

CADFLI microscopy was applied to capture images of the individual subsamples for visual segmentation of the reference MP fragments. Depending on the image resolution, 28 to 50 micrographs at a spatial resolution from 2.0 to 2.6 µm/pixel were merged using the Grid/collection stitching tool [23] to construct mosaics displaying the entire filter membrane (Figure 3).

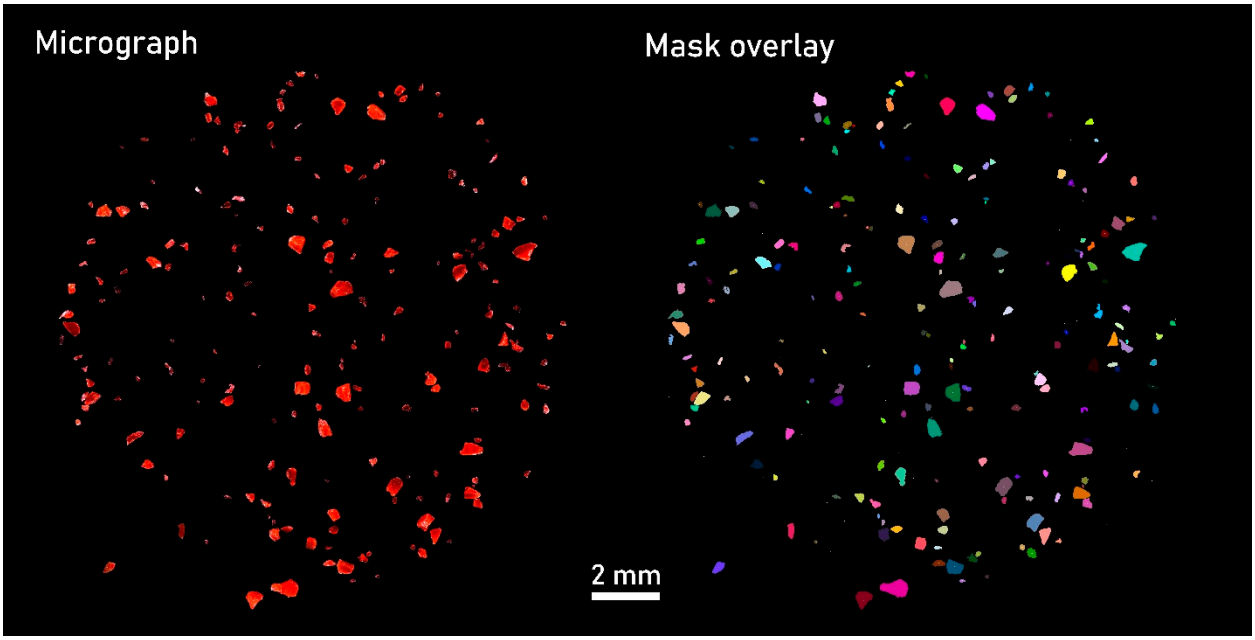


Figure 3. True-color micrograph mosaic captured under darkfield illumination at a spatial resolution of 2.6 µm/pixel, depicting subsample 1 of sample 1. 'Mask overlay' uses distinct colors to define individual MP particles.

This study presents a particle morphology to mass conversion formula (SFMM) where particle volume, and incidentally mass, is calculated on the basis of two observable 2D parameters: surface area (A), and minimum Feret diameter (F_{Min}). The volume (V) is calculated as the area of the particle multiplied by its height (h). Following the assumption that the observed lateral dimensions (y- and x-axis) are likely superior in length in comparison to the forward direction (z-axis or height), h is calculated as F_{Min} multiplied by the height multiplier (Figure 4). M_h is calibrated on the basis of the weighed mass of samples 1, 2, 3, 4 and 5.



Figure 4. Outlining of 2D particle morphology to volume conversion model (SFMM). (**A**) Determine minimum Feret diameter (F_{Min}). (**B**) The height (h) of the particle is determined as F_{Min} multiplied by the height multiplier M_h. (**C**) The volume (V) of the particle is determined as h multiplied by the surface area (**A**) of the particle. Graphic made with Inkscape.

Mass (m) is calculated by multiplying V by the specific gravity (ρ) of the polymer type in question, as per Equation (1):

$$m = \rho \cdot V = \rho \cdot (h \cdot A) = \rho \cdot ((M_h \cdot F_{Min}) \cdot A) \quad (1)$$

To calculate the optimal height multiplier for fragments, M_h was initially set to 1, which assumes particle height (h) equals the minimum Feret axis (F_{Min}). The ratio of weighed mass to the sum of calculated mass of all particles in the subsample determined the calibrated M_h for each individual subsample, as per Equation (2).

$$M_{h_{Calibrated}} = \frac{\sum m_{Calculated}}{m_{Weighed}} = \frac{\sum \rho \cdot ((M_h \cdot F_{Min}) \cdot A)}{m_{Weighed}} = \frac{\sum \rho \cdot ((1 \cdot F_{Min}) \cdot A)}{m_{Weighed}} \quad (2)$$

The current morphology to mass conversion equation is only applicable to particles with fragment-type morphology. However, in environmental settings, fragments constitute the majority of MPs found in natural samples; especially in the range of fine MPs < 100 µm in diameter [26–29].

3. Results and Discussion

3.1. Particle-Area Based Extrapolation

3.1.1. Sample-A

Within FOVs 1–4, a total of n = 7087, 16,754, 18,850, and 20,023 particles > 2 µm in area-equivalent diameter were segmented and analyzed by Raman microspectroscopy, respectively (Table 1). Here, n = 412, 751, 899, and 699 particles were identified as MPs, corresponding to 5.8%, 4.5%, 4.8% and 3.5% of the particle distribution, respectively. Although the total number of particles within individual FOVs varied by as much as n = 15 679 ± 5097 (33% RSD) (n = 4) the mean concentration of MPs remained more stable at 4.6% ± 0.8 (n = 4) (RSD = 18%).

The particle-area on the complete filter membrane was determined at 22.52 mm^2. Resultantly, FOVs 1–4 covered 2.84%, 2.01%, 2.85%, and 2.80% of the total particle-area, respectively, resulting in a mean particle-area coverage of 2.2% ± 0.72 per subsample.

Between the four investigated FOVs, the polymer type distribution remained consistent, with polyethylene (PE) making up 95.2% ± 1.1 (n = 4) of the polymer type distribution, followed by polyurethane (PU) at 2.0% ± 0.6 (n = 4) (Figure 5). Only 5 out of 12 detected polymer types were found in all four FOVs. Polymer types that comprised >0.5% of the relative distribution were detected in all four FOVs. The particle size distribution of detected MPs across the four FOVs remained stable with RSD values below 20% in most size groups.

Table 1. Particle count and surface area analysis for FOVs 1–4 of sample-A, showing generic particles, MP particles, area coverage ratios, and concentrations. N/A = not applicable.

Sample/Value	1 (TOP)	2 (LEFT)	3 (RIGHT)	4 (MID)	Mean	SD	RSD (%)
MP count (*n*)	412	751	899	699	690	177	25.6
Generic particle count (*n*)	7087	16,754	18,850	20,023	15,679	5097	32.5
MP count concentration (%)	5.8	4.5	4.8	3.5	4.6	0.8	17.8
MP area (μm^2)	2.77×10^4	4.97×10^4	7.68×10^4	5.85×10^4	N/A	N/A	N/A
Generic particle area (μm^2)	2.43×10^5	4.52×10^5	6.42×10^5	6.30×10^5	N/A	N/A	N/A
MPs (*n*) per generic particle area (μm^2)	0.0017	0.0017	0.0014	0.0011	0.0015	0.0002	16.0
MP area concentration (%)	11.4	11.0	12.0	9.3	10.9	1.0	9.1
Particle area full filter (μm^2)	2.25×10^7	2.25×10^7	2.25×10^7	2.25×10^7	N/A	N/A	N/A
Investigated particle area (%)	1.08	2.01	2.85	2.80	2.2	0.72	N/A

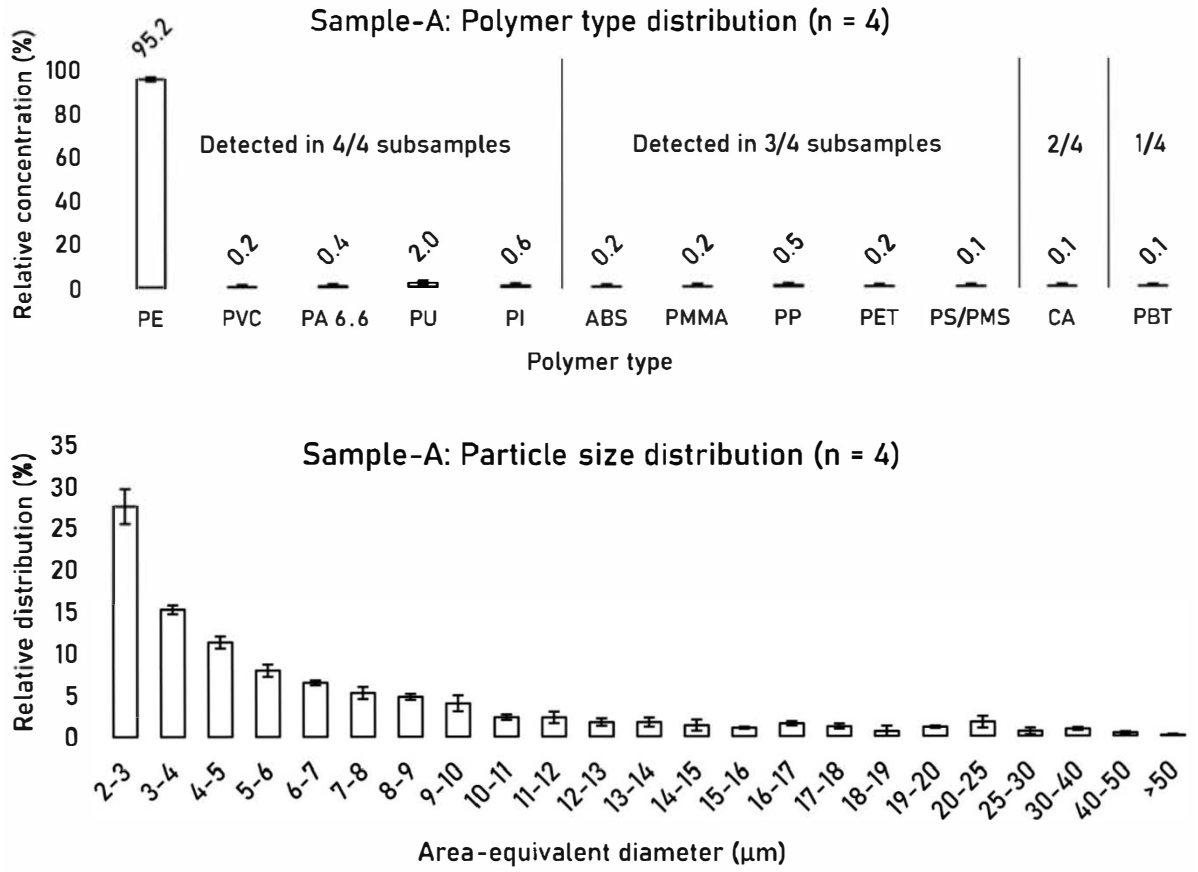


Figure 5. Relative polymer type distribution (**top**) and particle size distribution (PSD) (**bottom**) of detected MPs between FOVs 1–4 of sample-A.

3.1.2. Sample-B

Within FOVs 1–4, a total of n = 23,890, 13,616, 23,234, and 12,662 particles > 2 µm in area-equivalent diameter were segmented and analyzed by Raman microspectroscopy, respectively (Table 2). Here, n = 612, 364, 403, and 302 particles were identified as MPs, corresponding to 2.6%, 2.7%, 1.7% and 2.4% of the particle distribution, respectively. Although the total number of particles within individual FOVs varied by as much as n = 18 351 ± 5228 (29% RSD) (n = 4) the mean concentration of MPs remained more stable at 2.3% ± 0.4 (n = 4) (RSD = 16%).

Table 2. Particle count and surface area analysis for FOVs 1–4 of sample-B, showing generic particles, MP particles, area coverage ratios, and concentrations. N/A = not applicable.

Sample/Value	1 (TOP)	2 (LEFT)	3 (RIGHT)	4 (MID)	Mean	SD	RSD (%)
MP count (n)	620	364	403	302	422	120	28.4
Generic particle count (n)	23,890	13,616	23,234	12,662	18,351	5228	28.5
MP count concentration (%)	2.6	2.7	1.7	2.4	2.3	0.4	15.7
MP area (µm^2)	6.13×10^4	3.08×10^4	4.65×10^4	1.19×10^4	N/A	N/A	N/A
Generic particle area (µm^2)	6.38×10^5	3.40×10^5	5.82×10^5	4.77×10^5	N/A	N/A	N/A
MPs (n) per generic particle area (µm^2)	0.0010	0.0011	0.0007	0.0006	0.0008	0.0002	21.9
MP area concentration (%)	9.6	9.1	8.0	5.7	8.1	1.5	18.4
Particle area full filter (µm^2)	2.04×10^7	2.04×10^7	2.04×10^7	2.04×10^7	N/A	N/A	N/A
Investigated particle area (%)	3.14	1.67	2.86	2.34	2.5	0.56	N/A

The particle-area on the complete filter membrane was determined at 20.35 mm^2. Consequently, FOVs 1–4 covered 3.14%, 1.67%, 2.86%, and 2.34% of the total particle-area, respectively, resulting in a mean particle-area coverage of 2.5% ± 0.56 per subsample.

Between the four investigated FOVs, the polymer type distribution remained consistent, with PE constituting 85.6% ± 3.8 (n = 4) of the polymer type distribution, followed by PU at 7.5% ± 2.7 (n = 4) (Figure 6). 7 out of 13 detected polymer types were found in all four FOVs. Polymer types that comprised >0.5% of the relative distribution were detected in all four FOVs. The particle size distribution of detected MPs across the four FOVs remained relatively stable with the highest noticeable relative standard deviation (RSD) in the 2–3 µm fraction at 38% due to an outlying PSD profile of subsample 4.

3.2. Summary

For sample-A and sample-B the total number of particles within individual FOVs deviated by 33% and 29% RSD (n = 4) (Mean RSD = 31% [n = 8]), respectively, whereas relative MP concentrations were more stable at 18% (n = 4) and 16% RSD (n = 4), respectively (Mean RSD = 17% [n = 8]). This demonstrates that although particle spread on a filter membrane is heterogenous, the relative MP concentration remains relatively stable. Therefore, by establishing the MP concentration within a subsample, the total area of particles on a filter membrane can be used as a proxy for total MP count. These preliminary

results suggest that the current extrapolation technique is viable and may even outperform subsampling strategies such as 'random subsampling', 'random layout', and 'spiral layout' which demonstrated 50–80% error in FOVs with 2–5% sample coverage [6]. However, because the current extrapolation technique relies on the ratio between the number of MP particles and the area of generic particles, and not the number of generic particles, the extrapolation must be performed on this basis. The MP-to-generic-particle-area ratios for Sample-A and Sample-B were determined to be 0.0015 $n/\mu m^2 \pm 0.0002$ (RSD = 16%) and 0.0008 $n/\mu m^2 \pm 0.0002$ (RSD = 22%), respectively, with an average RSD of 19% (n = 8). This error is comparable to the 17% RSD observed in the particle-to-particle based MP concentration and is still lower than the overall particle spread of 31% RSD.

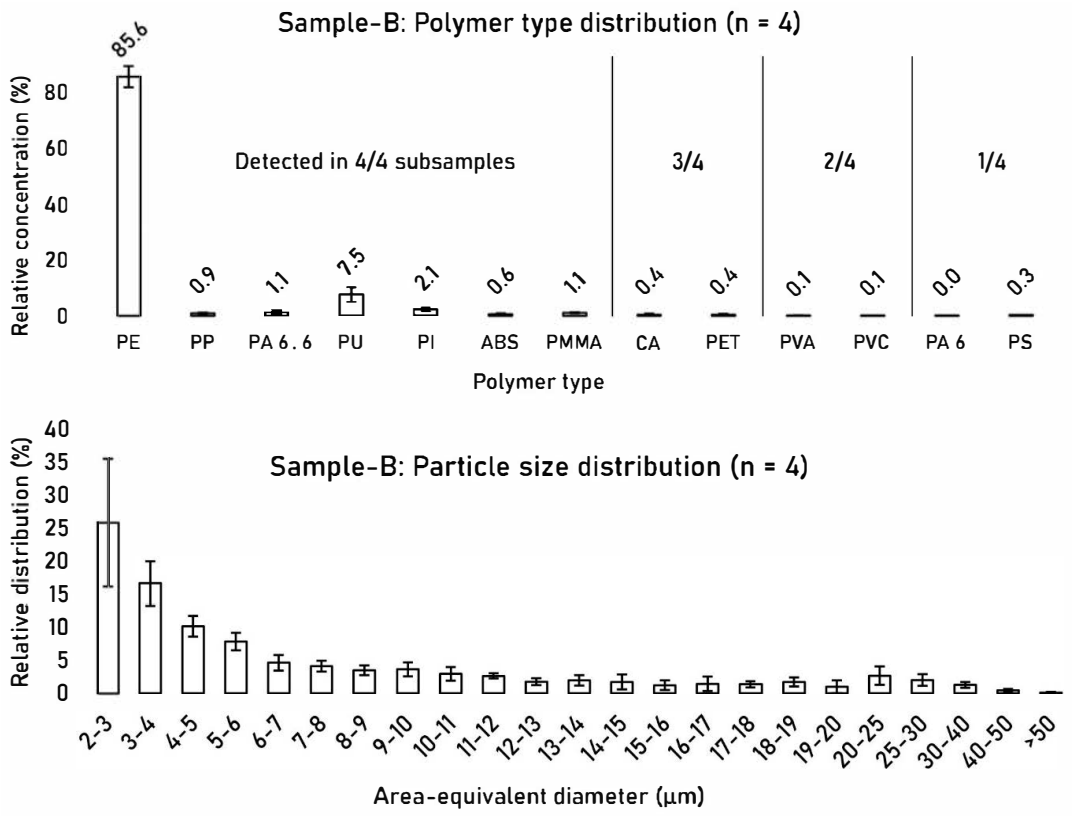


Figure 6. Relative polymer type distribution (**top**) and particle size distribution (PSD) (**bottom**) of detected MPs between FOVs 1–4 of sample-B.

3.2.1. Polymer Type and Particle Size Distribution

The relative polymer type distribution of detected MPs within the four FOVs remained relatively stable with close to negligible variation for both sample-A and sample-B. In both samples, any polymer type that exceeded 0.5% of the relative distribution was consistently detected in all four FOVs. The particle size distribution (PSD) in sample-A remained stable across all four FOVs. In contrast, sample-B exhibited greater PSD variation, particularly in the 2–3 µm fraction, with an RSD value of 38% due to subsample 4 being an outlier. To our knowledge, no previous extrapolation studies have reported performance data on the reproducibility of polymer type- or PSDs between FOVs. To achieve reproducibility values comparable to those in the current study, FOVs must include the analysis of at least 7000 particles [6], with at least 96 being MPs [30].

3.2.2. Data Comparability Despite Discrepancy Between Imaging Methods

By comparing the surface-area of the filter membrane covered by particles within individual FOVs to the total particle area of the filter, we estimated mean particle-area

coverage of 2.2% ± 0.7 (n = 4) for Sample-A and 2.5% ± 0.6 (n = 4) for sample-B. These values agree well with the theoretical filter coverage of 2.6% per 2 × 2 mm FOV (4 mm^2) within a circular filter of Ø = 1.4 cm (154 mm^2): 4 mm^2/154 mm^2·100 = 2.6%. These preliminary findings indicate that both imaging techniques provide consistent estimates of surface area coverage despite a difference in spatial resolution, i.e., 1 µm/pixel (Raman) vs. 2.6 µm/pixel (CADFLI). The observed consistency can be attributed to the fact that the relative particle size distribution remains stable across individual FOVs (Figure 7). This is important because although smaller particles may be missed or visually merged at lower resolution, the contribution of larger particles, which dominate total surface area, remains proportional to that of smaller ones. As a result, imaging the full membrane at lower resolution still yields a reliable estimate of overall coverage. Furthermore, particles < 5 µm accounted for only 10% (sample-A) and 17% (sample-B) of the total particle area (mean = 14%), suggesting that their omission or agglomeration in CADFLI microscopy has limited impact on area-based results. It was also found that the ratio between F_{Max} and particle surface area was highly comparable between the two techniques, although their particle size detection ranges differed. Raman imaging typically resolved particles up to ~40 µm, whereas ColSpec captured particles up to ~400 µm, with most falling between 20 and 60 µm. Consequently, while ColSpec is unsuitable for determining absolute counts of very fine particles due to visual agglomeration, it still provides sufficiently accurate estimates of total particle surface area coverage. Our investigation is still preliminary, so exact error quantification is not yet possible. Still, the results show good overall agreement, with only minor bias from missing very fine particles at lower resolution, suggesting the approach is promising.

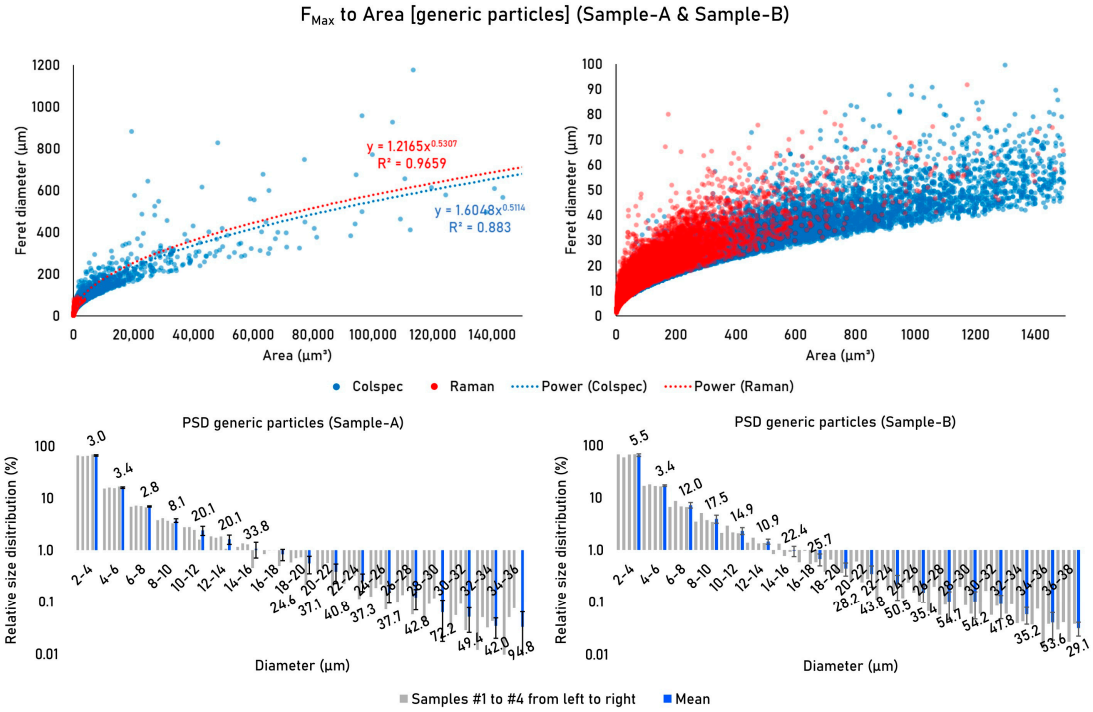


Figure 7. (**Top**) Comparison of the ratio between F_{Max} and particle surface area obtained by Raman and ColSpec imaging. Both methods show good agreement, although Raman did not capture larger particles that were resolved by ColSpec. (**Bottom**) Relative particle size distributions based on Raman imaging across four subsamples from samples A and B. Values indicate relative standard deviation of PSD within size groups. The relatively stable distributions indicate that the surface area of larger particles reliably reflects that of smaller ones, allowing the surface area of larger particles to be used as a proxy for the total surface area and, by extension, the abundance of smaller particles.

3.3. Two-Dimensional Particle Morphology to Mass Conversion Model

Calibration of the height multiplier (M_h) was performed with data from twenty weighed subsamples shown in Figure 8, covering MP fragments ranging from 10 µm to 1500 µm (1.5 mm) in diameter.

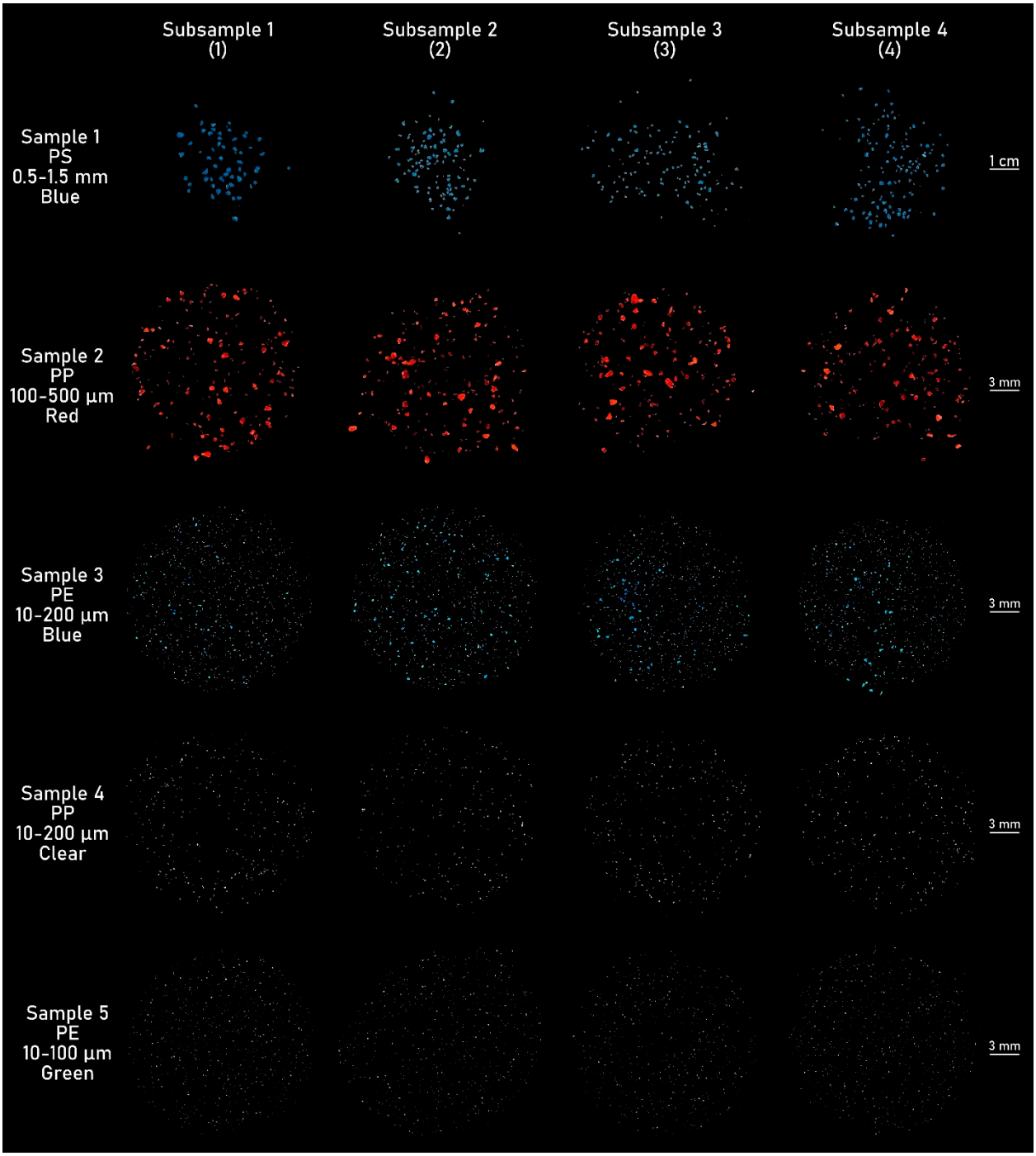


Figure 8. Micrograph mosaics captured under darkfield illumination of subsamples 1–4 from samples 1–5 (20 subsamples total), showing MP fragments spanning 10 µm to 1500 µm (1.5 mm) in Feret diameter.

Calibrated M_h values for individual subsamples are listed in Table 3. Across 20 subsamples, M_h ranged from 0.26 to 0.47 with a mean value of 0.34 ± 0.05 (15% RSD) (Figure 9). The

SFMM calculates MP fragment mass from 2D morphological data by applying a simplified 3D model where particle height equals one third (0.34) of the minimum Feret axis (F_{Min}).

Table 3. Summary data for investigated subsamples including weighed mass, calibrated height multiplier (M_h), number of MP particles, and particle size range. N/A = not applicable.

Sample	Weighed Mass (µg)	Calibrated Height Multiplier (M_h) as per Equation (2)	Number of Particles (n)	Size Range (µm)
1(1)	17,400	0.376	57	500–1500
1(2)	20,400	0.369	102	500–1500
1(3)	14,000	0.321	118	500–1500
1(4)	23,400	0.305	133	500–1500
2(1)	1042	0.311	207	100–500
2(2)	1042	0.311	214	100–500
2(3)	1042	0.330	193	100–500
2(4)	1042	0.381	200	100–500
3(1)	198	0.466	6344	10–200
3(2)	198	0.319	5205	10–200
3(3)	198	0.284	5246	10–200
3(4)	198	0.304	5438	10–200
4(1)	63.3	0.316	571	10–200
4(2)	63.3	0.263	505	10–200
4(3)	63.3	0.308	524	10–200
4(4)	63.3	0.330	492	10–200
5(1)	54	0.346	3140	10–100
5(2)	54	0.466	3179	10–100
5(3)	54	0.368	2740	10–100
5(4)	54	0.401	3172	10–100
Mean	N/A	0.344	N/A	N/A
SD	N/A	0.053	N/A	N/A
RSD (%)	N/A	15.4	N/A	N/A

In conclusion, the mass of a MP fragment can be calculated on the basis of F_{Min} and surface area (A) alone, assuming a particle height equating to approximately one third (0.34) of F_{Min} as per Equation (3).

$$m = \rho \cdot ((M_h \cdot F_{Min}) \cdot A) = \rho \cdot ((0.34 \cdot F_{Min}) \cdot A) \quad (3)$$

However, published morphological data such as F_{Min} and area are rarely provided in environmental datasets, whereas F_{Max} is more commonly reported [31,32]. Therefore, an alternative formula for calculating particle volume based on F_{Max} instead of F_{Min} is proposed here. The ratio between F_{Min} and F_{Max} was determined for all investigated particles within each subsample (Figure 10).

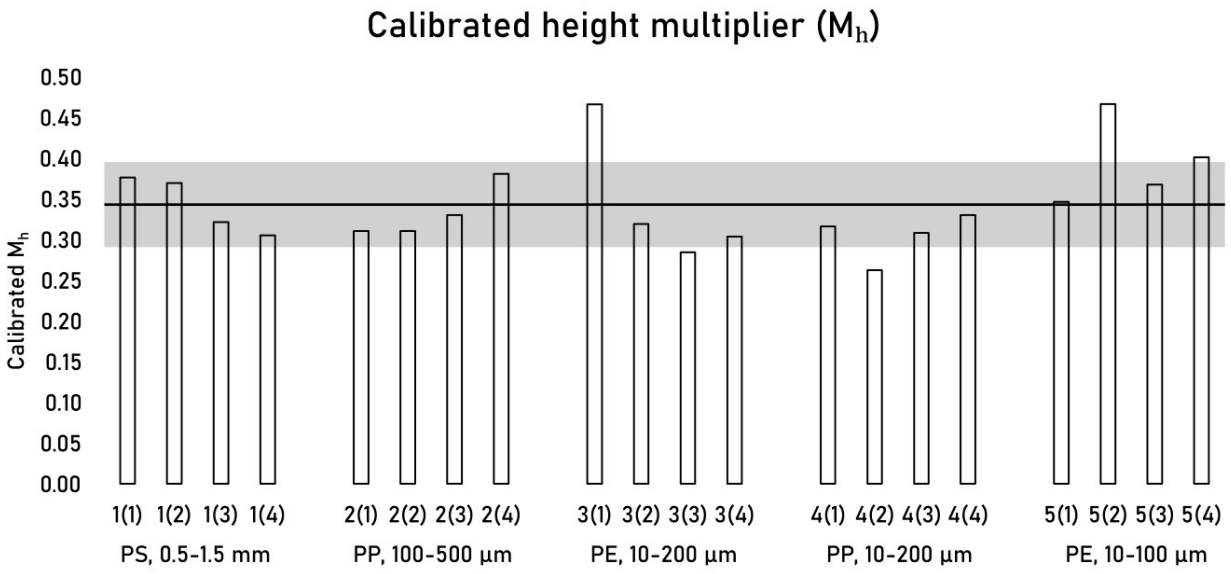


Figure 9. Height multiplier (M_h) calibration results for subsamples 1–4 from samples 1–5 (n = 20). Sample identification: 1(2) denotes subsample 2 of sample 1. The solid black line represents the mean M_h (0.34), and the grey bar indicates ± the standard deviation (0.05).

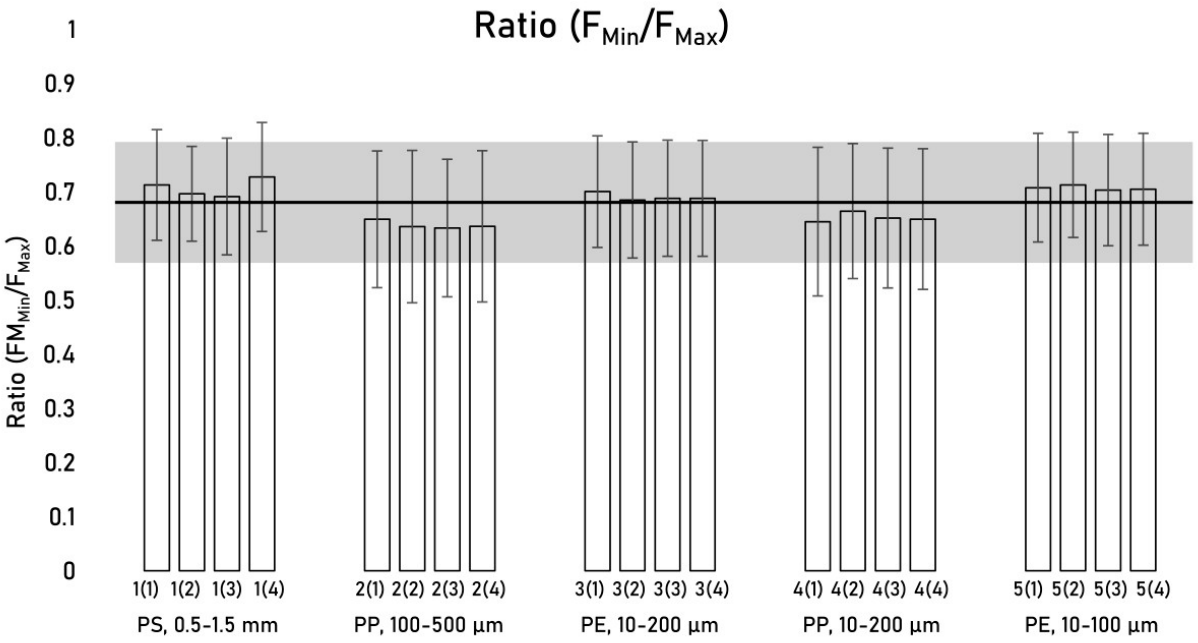


Figure 10. Mean F_{Min}/F_{Max} ratios within individual subsamples. Sample identification: 1(2) denotes subsample 2 of sample 1. The error bars represent the standard deviation within the individual subsamples. The solid black line represents the mean F_{Min}/F_{Max} ratio (0.68), and the grey bar indicates ± the overall standard deviation (0.11).

Between all particles in individual subsamples, the F_{Min}/F_{Max} ratio was determined to be 0.68 ± 0.11 (17% RSD) [n = 37,780], demonstrating fair coherency between the minor and major axis of MP fragments.

Similar F_{Min}/F_{Max} ratios of 0.67 ± 0.22 were reported for environmental MP in the 10–300 µm range [19], and 0.67 for particles and fibers from multiple aquatic compartments [3]. We are then able to calibrate a single proportionality constant, k_h, for particle height relative to F_{Min} in the classical ellipsoid volume expression:

$$V = \frac{4}{3}\pi \cdot \frac{F_{Max}}{2} \cdot \frac{0.68 \cdot F_{Max}}{2} \cdot \frac{k_h \cdot 0.68 \cdot F_{Max}}{2} \quad (4)$$

Based on the 20 individual subsamples of varying MP range, we find that $k_h = 0.40 \pm 0.08$ (SD; 20% RSD), We note that k_h varies randomly as a function of particle size range, and number of particles counted. By combining all the various constants in Equation (4), including π, into a single constant ($4/3 \cdot \pi \cdot 1/2 \cdot 1/2 \cdot 1/2 \cdot 0.68 \cdot 0.40 \cdot 0.68 = 0.097$), we can express a simplified MP fragment mass approximation, for cases where only the length estimator F_{Max} is reported:

$$m = \rho \cdot 0.097 \cdot (F_{Max})^3 \quad (5)$$

Previous studies have assumed k_h to be identical to F_{Min}/F_{Max}, i.e., around 0.67 [33,34]. Our lower calibrated k_h value of 0.40 leads to a 40% ([0.67 − 0.40/0.67]) lower volume and mass estimate for each small MP fragment. It is of interest to note that our final volume expression in Equation (5), $V = 0.097 \cdot (F_{Max})^3$, is identical within the overall combined uncertainty of the constant, 0.097 ± 0.032 (33% RSD) to the volume expression for a flat-shaped ellipse assumed by Cozar et al. [34]: $V = 0.1 \cdot (L)^3$, where L = particle length (F_{Max} here in this study). The SFMM equation (Equation (5)) provides a practical alternative for when only F_{Max} measurements are available. However, because it introduces an additional layer of uncertainty it should only be used when F_{Min} and area are unavailable.

3.4. Limitations

3.4.1. Particle-Area Based Extrapolation

Matrix-Specific Effects

The area-based extrapolation technique was validated using Sphagnum moss samples, which may not represent the particle distribution patterns found in other environmental matrices such as sediments, marine waters, or urban runoff. Different sample types may exhibit varying degrees of particle aggregation or settling behavior that could affect extrapolation accuracy.

Instrumental Limitations

The spatial resolution differences between Raman microspectroscopy (0.3 µm/pixel) [effectively ~1 µm/pixel] and CADFLI microscopy (2.6 µm/pixel) may introduce systematic errors in area measurements, particularly for smaller particles approaching the detection limits of either technique. More sensitive techniques may be required for full filter imaging of less charged filters, where particle density is insufficient for reliable darkfield visualization and accurate area quantification.

3.4.2. Two-Dimensional Morphology-To-Mass Conversion Model

Polymer Density

Mass calculations require accurate polymer density values, which may vary between virgin and weathered MPs. Environmental microplastics may have altered densities due to biofilm formation, photodegradation, or additive leaching, potentially affecting mass estimates [35–37]. However, it should be noted that while weathering processes may change the current measured density of particles, the calculations still represent the original plastic mass released into the environment, which is the fundamental parameter needed for environmental impact assessments and plastic flux modeling.

MP Morphology

The current model is calibrated using data from artificially generated microplastic (MP) fragments and should therefore only be applied to samples in which fragments represent the dominant MP type. Notably, most environmental MPs smaller than 50 µm exhibit fragment-type morphology, as they primarily arise from the fragmentation of larger

plastics [38,39]. Accordingly, the SFMM is best suited for fine MP samples or for samples with larger MPs in which fragments predominate.

4. Conclusions and Perspectives

This study presents two methodological advances for environmental microplastic analysis: an area-based extrapolation technique for organic-rich samples and a simplified morphology-to-mass conversion model (SFMM). The area-based extrapolation technique uses MP-to-generic particle area ratios rather than particle counts for extrapolation. While total particle distribution varied considerably (31% RSD [n = 8]), MP concentrations showed greater stability (17% RSD [n = 8]). The method achieved reliable extrapolation from ~2.6% mean filter coverage, outperforming existing subsampling strategies that report 50–80% error rates in the 2–5 µm size range. Polymer types that constituted > 0.5% of the distribution were consistently detected across all fields of view (FOVs). The SFMM converts 2D morphological data to mass estimates using surface area and minimum Feret diameter. Calibration across 20 reference material subsamples, using MP fragments ranging from 10 to 1500 µm in diameter, yielded a height multiplier of 0.34 ± 0.05 (15% RSD), establishing that fragment height equals approximately one-third of the minimum Feret diameter for this simplified plane-particle model. The model is applicable to fragment-type particles only as per the following equation:

$$m = \rho \cdot ((M_h \cdot F_{Min}) \cdot A) = \rho \cdot ((0.34 \cdot F_{Min}) \cdot A)$$

where m is mass, ρ is the specific gravity of the relevant polymer, M_h is the height multiplier calibrated to be 0.34, A is the surface area, and F_{Min} is the minimum Feret axis of the particle. An alternative equation is provided for when F_{Min} is unavailable, using maximum Feret axis (F_{Max}). These methods provide practical advantages for routine environmental monitoring: reduced analysis time, direct mass estimation capability, and compatibility with existing spectroscopic workflows. Ideally the new volume and mass parameterizations can be intercompared directly with direct mass-based techniques such as pyrolysis GC-MS.

Supplementary Materials: The following supporting information can be downloaded at: https://www.mdpi.com/article/10.3390/microplastics4040080/s1.

Author Contributions: O.H. conceptualized and administered the project, and led the laboratorial work. O.H. and J.E.S. interpreted data and led manuscript writing with help from H.M. and N.Y. J.E.S. and G.l.R. secured part of the funding and provided critical revision of the manuscript. All authors have read and agreed to the published version of the manuscript.

Funding: This work is funded by Microplastic Solution (MPS). Raman analyses were funded by an 80Prime CNRS grant «4DµPlast» (G.l.R., J.E.S.) and supported by ANR-20-CE34-0014 ATMO-PLASTIC (G.l.R, J.E.S.), ANR-23-CE34-0012 BUBBLEPLAST (J.E.S.) and the Plasticopyr project (G.l.R.) within the Interreg V-A Spain-France-Andorra program (G.l.R.) as well as observatoire Homme-Milieu Pyrénées Haut Vicdessos—LABEX DRIIHM ANR-11-LABX0010 (G.l.R.).

Data Availability Statement: All data will be made available upon request.

Acknowledgments: We thank Jeremy M. Lerner and LightForm® Inc. for their ongoing technical support.

Conflicts of Interest: Oskar Hagelskjær, Henar Margenat, and Nadiia Yakovenko were employed by the company Microplastic Solution; Jeroen E. Sonke and Gaël Le Roux are the scientific advisors of Microplastic Solution (non-profit).

Abbreviations

The following abbreviations are used in this manuscript:

MP	Microplastic
n	Number of particles
SD	Standard deviation
RSD	Relative standard deviation
M_h	Height multiplier
k_h	Proportionality constant for particle height relative to F_{Min}
m	Mass
h	Height
A	Area
V	Volume
FOV	Field of view
CADFLI	Critical angle darkfield illumination
F_{Min}	Minimum Feret diameter
F_{Max}	Maximum Feret diameter
PE	Polyethylene
PP	Polypropylene
PS	Polystyrene

References

1. El Khatib, D.; Langknecht, T.D.; Cashman, M.A.; Reiss, M.; Somers, K.; Allen, H.; Ho, K.T.; Burgess, R.M. Assessment of filter subsampling and extrapolation for quantifying microplastics in environmental samples using Raman spectroscopy. *Mar. Pollut. Bull.* **2023**, *192*, 115073. [CrossRef]
2. *ISO 24187*; 2023 Principles for the Analysis of Microplastics Present in the Environment. International Organization for Standardization: Geneva, Switzerland, 2023. Available online: https://www.iso.org/standard/78033.html (accessed on 1 October 2025).
3. *ISO/FDIS 16094-2*; Water Quality—Analysis of Microplastic in Water: Part 2: Vibrational Spectroscopy Methods for Waters with Low Content of Suspended Solids Including Drinking Water. ISO: Geneva, Switzerland, 2025. Available online: https://www.iso.org/standard/84460.html (accessed on 1 April 2025).
4. Hagelskjær, O.; Hagelskjær, F.; Margenat, H.; Yakovenko, N.; Sonke, J.E.; Le Roux, G. Majority of potable water microplastics are smaller than the 20 µm EU methodology limit for consumable water quality. *PLoS Water* **2025**, *4*, 1–14.
5. Hagelskjær, O.; Le Roux, G.; Liu, R.; Dubreuil, B.; Behra, P.; Sonke, J.E. The recovery of aerosol-sized microplastics in highly refractory vegetal matrices for identification by automated Raman microspectroscopy. *Chemosphere* **2023**, *328*, 138487. [CrossRef] [PubMed]
6. Brandt, J.; Fischer, F.; Kanaki, E.; Enders, K.; Labrenz, M.; Fischer, D. Assessment of Subsampling Strategies in Microspectroscopy of Environmental Microplastic Samples. *Front. Environ. Sci.* **2021**, *8*, 579676. Available online: https://www.frontiersin.org/journals/environmental-science/articles/10.3389/fenvs.2020.579676 (accessed on 1 April 2025). [CrossRef]
7. Thaysen, C.; Munno, K.; Hermabessiere, L.; Rochman, C.M. Towards Raman Automation for Microplastics: Developing Strategies for Particle Adhesion and Filter Subsampling. *Appl. Spectrosc.* **2020**, *74*, 976–988. [CrossRef]
8. De Frond, H.; O'Brien, A.M.; Rochman, C.M. Representative subsampling methods for the chemical identification of microplastic particles in environmental samples. *Chemosphere* **2023**, *310*, 136772. [CrossRef]
9. Huppertsberg, S.; Knepper, T.P. Instrumental analysis of microplastics—Benefits and challenges. *Anal. Bioanal. Chem.* **2018**, *410*, 6343–6352. [CrossRef]
10. Everaert, G.; Van Cauwenberghe, L.; De Rijcke, M.; Koelmans, A.A.; Mees, J.; Vandegehuchte, M.; Janssen, C.R. Risk assessment of microplastics in the ocean: Modelling approach and first conclusions. *Environ. Pollut.* **2018**, *242*, 1930–1938. [CrossRef]
11. Gouin, T.; Becker, R.A.; Collot, A.; Davis, J.W.; Howard, B.; Inawaka, K.; Lampi, M.; Serrano Ramon, B.; Shi, J.; Hopp, P.W. Toward the Development and Application of an Environmental Risk Assessment Framework for Microplastic. *Environ. Toxicol. Chem.* **2019**, *38*, 2087–2100. [CrossRef]
12. Thompson, R.C.; Courtene-Jones, W.; Boucher, J.; Pahl, S.; Raubenheimer, K.; Koelmans, A.A. Twenty years of microplastics pollution research—What have we learned? *Science* **2024**, *386*, eadl2746. [CrossRef] [PubMed]

13. Huang, Z.; Hu, B.; Wang, H. Analytical methods for microplastics in the environment: A review. *Environ. Chem. Lett.* **2023**, *21*, 383–401. [CrossRef]
14. Lykkemark, J.; Mattonai, M.; Vianello, A.; Gomiero, A.; Modugno, F.; Vollertsen, J. Py–GC–MS analysis for microplastics: Unlocking matrix challenges and sample recovery when analyzing wastewater for polypropylene and polystyrene. *Water Res.* **2024**, *261*, 122055. [CrossRef]
15. Yang, Z.; Nagashima, H.; Arakawa, H. Development of automated microplastic identification workflow for Raman micro-imaging and evaluation of the uncertainties during micro-imaging. *Mar. Pollut. Bull.* **2023**, *193*, 115200. [CrossRef]
16. Barchiesi, M.; Kooi, M.; Koelmans, A.A. Adding Depth to Microplastics. *Environ. Sci. Technol.* **2023**, *57*, 14015–14023. [CrossRef]
17. Contreras, L.; Edo, C.; Rosal, R. Mass concentration of plastic particles from two-dimensional images. *Sci. Total Environ.* **2024**, *946*, 173849. [CrossRef]
18. Kataoka, T.; Iga, Y.; Baihaqi, R.A.; Hadiyanto, H.; Nihei, Y. Geometric relationship between the projected surface area and mass of a plastic particle. *Water Res.* **2024**, *261*, 122061. [CrossRef] [PubMed]
19. Simon, M.; van Alst, N.; Vollertsen, J. Quantification of microplastic mass and removal rates at wastewater treatment plants applying Focal Plane Array (FPA)-based Fourier Transform Infrared (FT-IR) imaging. *Water Res.* **2018**, *142*, 1–9. [CrossRef]
20. Almádi, G.; MacG. Dawson, R.J.; Domokos, G.; Regős, K. On Equilibria of Tetrahedra. *Math. Intell.* **2023**, *46*, 247–254. [CrossRef]
21. Munno, K.; De Frond, H.; O'Donnell, B.; Rochman, C.M. Increasing the Accessibility for Characterizing Microplastics: Introducing New Application-Based and Spectral Libraries of Plastic Particles (SLoPP and SLoPP-E). *Anal. Chem.* **2020**, *92*, 2443–2451. [CrossRef] [PubMed]
22. Cabernard, L.; Roscher, L.; Lorenz, C.; Gerdts, G.; Primpke, S. Comparison of Raman and Fourier Transform Infrared Spectroscopy for the Quantification of Microplastics in the Aquatic Environment. *Environ. Sci. Technol.* **2018**, *52*, 13279–13288. [CrossRef]
23. Preibisch, S.; Saalfeld, S.; Tomancak, P. Globally optimal stitching of tiled 3D microscopic image acquisitions. *Bioinformatics* **2009**, *25*, 1463–1465. [CrossRef]
24. Hagelskjær, O.; Hagelskjær, F.; Margenat, H.; Sonke, J.E.; Roux, G.L. EasyMP: Diverse and Environmentally Relevant Microplastic Reference Materials Encompassing Fragments and Fibers. *Nano. Sel.* **2025**, *6*, e70004. [CrossRef]
25. McColley, C.J.; Nason, J.A.; Harper, B.J.; Harper, S.L. An assessment of methods used for the generation and characterization of cryomilled polystyrene micro- and nanoplastic particles. *Microplastics Nanoplastics* **2023**, *3*, 20. [CrossRef]
26. Allen, D.; Allen, S.; Le Roux, G.; Simonneau, A.; Galop, D.; Phoenix, V.R. Temporal Archive of Atmospheric Microplastic Deposition Presented in Ombrotrophic Peat. *Environ. Sci. Technol. Lett.* **2021**, *8*, 954–960. [CrossRef]
27. Boettcher, H.; Kukulka, T.; Cohen, J.H. Methods for controlled preparation and dosing of microplastic fragments in bioassays. *Sci. Rep.* **2023**, *13*, 5195. [CrossRef]
28. Velasco, A.d.J.N.; Rard, L.; Blois, W.; Lebrun, D.; Lebrun, F.; Pothe, F.; Stoll, S. Microplastic and Fibre Contamination in a Remote Mountain Lake in Switzerland. *Water* **2020**, *12*, 2410. [CrossRef]
29. Stefánsson, H.; Peternell, M.; Konrad-Schmolke, M.; Hannesdóttir, H.; Ásbjörnsson, E.J.; Sturkell, E. Microplastics in Glaciers: First Results from the Vatnajökull Ice Cap. *Sustainability* **2021**, *13*, 4183. [CrossRef]
30. Cowger, W.; Markley, L.; Moore, S.; Gray, A.; Upadhyay, K.; Koelmans, A. How Many Microplastics Do You Need to (Sub)Sample? *Ecotoxicol. Environ. Saf.* **2023**, *275*, 116243. [CrossRef] [PubMed]
31. Sonke, J.E.; Koenig, A.; Segur, T.; Yakovenko, N. Global environmental plastic dispersal under OECD policy scenarios toward 2060. *Sci. Adv.* **2025**, *11*, eadu2396. [CrossRef]
32. Sonke, J.E.; Koenig, A.M.; Yakovenko, N.; Hagelskjær, O.; Margenat, H.; Hansson, S.V.; De Vleeschouwer, F.; Magand, O.; Le Roux, G.; Thomas, J.L. A mass budget and box model of global plastics cycling, degradation and dispersal in the land-ocean-atmosphere system. *Microplastics Nanoplastics* **2022**, *2*, 1–14. [CrossRef]
33. Kooi, M.; Primpke, S.; Mintenig, S.M.; Lorenz, C.; Gerdts, G.; Koelmans, A. Characterizing the multidimensionality of microplastics across environmental compartments. *Water Res.* **2021**, *202*, 117429. [CrossRef] [PubMed]
34. Cózar, A.; Echevarría, F.; González-Gordillo, J.I.; Irigoien, X.; Úbeda, B.; Hernández-León, S.; Palma, Á.T.; Navarro, S.; García-de-Lomas, J.; Ruiz, A.; et al. Plastic debris in the open ocean. *Proc. Natl. Acad. Sci. USA* **2014**, *111*, 10239–10244. [CrossRef]
35. Jansen, M.A.K.; Andrady, A.L.; Bornman, J.F.; Aucamp, P.J.; Bais, A.F.; Banaszak, A.T.; Barnes, P.W.; Bernhard, G.H.; Bruckman, L.S.; Busquets, R.; et al. Plastics in the environment in the context of UV radiation, climate change and the Montreal Protocol: UNEP Environmental Effects Assessment Panel, Update 2023. *Photochem. Photobiol. Sci.* **2024**, *23*, 629–650. [CrossRef]
36. Moyal, J.; Dave, P.H.; Wu, M.; Karimpour, S.; Brar, S.K.; Zhong, H.; Kwong, R.W. Impacts of Biofilm Formation on the Physicochemical Properties and Toxicity of Microplastics: A Concise Review. *Rev. Environ. Contam. Toxicol.* **2023**, *261*, 8. [CrossRef]

37. Yu, W.; Wen, Q.; Yang, J.; Xiao, K.; Zhu, Y.; Tao, S.; Lv, Y.; Liang, S.; Fan, W.; Zhu, S.; et al. Unraveling oxidation behaviors for intracellular and extracellular from different oxidants (HOCl vs. H_2O_2) catalyzed by ferrous iron in waste activated sludge dewatering. *Water Res.* **2019**, *148*, 60–69. [CrossRef] [PubMed]
38. Hagelskjær, O.; Crézé, A.; Le Roux, G.; Sonke, J.E. Investigating the correlation between morphological features of microplastics (5–500 μm) and their analytical recovery. *Microplastics Nanoplastics* **2023**, *3*, 22. [CrossRef]
39. Chamas, A.; Moon, H.; Zheng, J.; Qiu, Y.; Tabassum, T.; Jang, J.H.; Abu-Omar, M.; Scott, S.L.; Suh, S. Degradation Rates of Plastics in the Environment. *ACS Sustain. Chem. Eng.* **2020**, *8*, 3494–3511. [CrossRef]

Disclaimer/Publisher's Note: The statements, opinions and data contained in all publications are solely those of the individual author(s) and contributor(s) and not of MDPI and/or the editor(s). MDPI and/or the editor(s) disclaim responsibility for any injury to people or property resulting from any ideas, methods, instructions or products referred to in the content.